

Towards high-speed computational scattered light imaging by introducing compressed sensing for optimized illumination

Auf Der Heiden, Franca; Münzer, Oliver; Van Staalduine, Simon; Amunts, Katrin; Axer, Markus; Menzel, Miriam

DOI

[10.1117/12.3000869](https://doi.org/10.1117/12.3000869)

Publication date

2024

Document Version

Final published version

Published in

High-Speed Biomedical Imaging and Spectroscopy IX

Citation (APA)

Auf Der Heiden, F., Münzer, O., Van Staalduine, S., Amunts, K., Axer, M., & Menzel, M. (2024). Towards high-speed computational scattered light imaging by introducing compressed sensing for optimized illumination. In K. K. Tsia, & K. Goda (Eds.), *High-Speed Biomedical Imaging and Spectroscopy IX* Article 1285303 (Progress in Biomedical Optics and Imaging - Proceedings of SPIE; Vol. 12853). SPIE. <https://doi.org/10.1117/12.3000869>

Important note

To cite this publication, please use the final published version (if applicable). Please check the document version above.

Copyright

Other than for strictly personal use, it is not permitted to download, forward or distribute the text or part of it, without the consent of the author(s) and/or copyright holder(s), unless the work is under an open content license such as Creative Commons.

Takedown policy

Please contact us and provide details if you believe this document breaches copyrights. We will remove access to the work immediately and investigate your claim.

Towards High-speed Computational Scattered Light Imaging by Introducing Compressed Sensing for Optimized Illumination

Franca auf der Heiden^a, Oliver Münzer^a, Simon van Staalduine^b, Katrin Amunts^a, Markus Axer^a, and Miriam Menzel^{a, b}

^aInstitute of Neuroscience and Medicine, Forschungszentrum Jülich GmbH, 52425 Jülich, DE

^bDepartment of Imaging Physics, Delft University of Technology, 2628 CJ Delft, NL

ABSTRACT

We propose the application of Compressed Sensing to Computational Scattered Light Imaging to decrease measurement time and data storage. Computational Scattered Light Imaging (ComSLI) determines three-dimensional fiber orientations and crossings in biomedical tissues like brain tissue. Currently, conventional ComSLI is time-consuming and generates large data. Compressed Sensing reconstructs signals with fewer samples than required by the Shannon-Nyquist theorem with minimal perceptual loss, significantly reducing the number of measurements. We introduce an optimized illumination strategy for ComSLI based on the Discrete Cosine Transform and validate it by reconstructing characteristic scattering patterns in vervet brain tissue, thereby demonstrating the feasibility of Compressed Sensing in ComSLI.

Keywords: Scattered Light Imaging, Scatterometry, Neuroimaging, Brain Structure, White Matter, Nerve Fibers, Compressed Sensing, Discrete Cosine Transform

1. INTRODUCTION

The nerve fiber architecture in post-mortem brain sections can be mapped using Computational Scattered Light Imaging (ComSLI), a novel imaging technique introduced by Menzel et al¹ that exploits scattering properties of fibrous tissue. In particular, ComSLI can determine nerve fiber orientations from densely packed white matter with a micrometer resolution and can not only resolve single fiber tract orientations, but also fiber crossings. Previous experiments have shown that ComSLI yields meaningful results for a variety of tissue types and stains.² When light passes vertically through fibrous tissue and the wavelength is of approximately the diameter of the fibers (i.e., light in the visible spectrum for nerve fibers), a scattering pattern emerges for every image pixel, containing information about the three-dimensional fiber orientations and crossings³. In ComSLI, the light path is flipped: By illuminating the whole sample at once but under different angles (i.e., square by square in an $N \times N$ grid of illumination squares), the scattering patterns for every image pixel can be reconstructed from the $N \times N$ measurement images.⁴

However, ComSLI scatterometry is time-consuming: With a typical exposure time of about one second per illumination square and a typical gridsize of 64×64 squares, the measurement of one image set already takes more than an hour, yet without regard to data processing of the measurement hardware. Furthermore, ComSLI scatterometry produces huge amounts of data with up to 100GB per image set. Therefore, it is crucial to reduce both the measurement time and the amount of saved data. Compressed Sensing is a promising approach to reduce the amount of required ComSLI measurements significantly by illuminating the sample not square by square, but with a reduced number of selected illumination images. In this paper, we show that Compressed Sensing can be applied to ComSLI. We develop the mathematical background for Compressed Sensing in ComSLI and perform first measurements on vervet brain tissue as a proof-of-concept.

Further author information:

E-mail: f.auf.der.heiden@fz-juelich.de

2. MATHEMATICAL BACKGROUND

2.1 Compressed Sensing

Compressed Sensing allows the reconstruction of a signal with fewer single images than required by the Shannon-Nyquist theorem under the condition that the signal is sparse.⁵ Furthermore, it has been shown that approximately sparse signals, i.e. compressible signals, can also be nearly recovered. By following a non-linear method called "Compressed Sensing" and performing a set of those measurements that have the highest impact on the recovery of the actual signal, measurement efforts can be reduced drastically with no or little perceptual loss.⁶

In ComSLI, this condition is fulfilled: The illumination images can be understood as matrices with a gridsize $N \times N$ that contains only zeros except for one non-zero entry, representing the single illuminated square (compare Fig. 1b)). Those $N \times N$ matrices form a mathematical basis and will be referred to as "Euclidean illumination" in the following. To obtain a different orthogonal set of matrices that is compressible, the original matrices are transformed into the frequency domain by applying a Discrete Cosine Transformation (DCT) of type II (DCT-II).^{7,8} The DCT-II is defined as:

$$f_0 = \frac{\sqrt{2}}{N} \sum_{n=0}^{N-1} x_n \quad (1)$$

$$f_k = \frac{2}{N} \sum_{n=0}^{N-1} x_n \cos \left[\frac{\pi}{N} \left(n + \frac{1}{2} \right) k \right] \quad \text{for } k = 1, \dots, N-1 \quad (2)$$

In two dimensions, this reads as:

$$X_{k_1, k_2} = \sum_{n_1=0}^{N_1-1} \left(\sum_{n_2=0}^{N_2-1} x_{n_1, n_2} \cos \left[\frac{\pi}{N_2} \left(n_2 + \frac{1}{2} \right) k_2 \right] \right) \cos \left[\frac{\pi}{N_1} \left(n_1 + \frac{1}{2} \right) k_1 \right] \quad (3)$$

$$= \sum_{n_1=0}^{N_1-1} \sum_{n_2=0}^{N_2-1} x_{n_1, n_2} \cos \left[\frac{\pi}{N_1} \left(n_1 + \frac{1}{2} \right) k_1 \right] \cos \left[\frac{\pi}{N_2} \left(n_2 + \frac{1}{2} \right) k_2 \right]. \quad (4)$$

The obtained matrices represent $N \times N$ new illumination images characterized by periodic fluctuations in intensity (different gray values) with increasing frequency. It is important to note that these matrices may contain both positive and negative entries. Light intensity can inherently only take positive values; therefore the positive and the negative part of the matrix are measured separately, resulting in two illumination matrices per transformed matrix. This approach may appear counter-intuitive since it doubles the number of required measurements. However, during Compressed Sensing, only the low-frequency illumination matrices need to be measured, such as the lowest $2 \times 8 \times 8$ coefficients in a 64×64 grid. Assuming the signal is compressible, higher coefficients can be assumed to be zero. Therefore, this approach is still beneficial, reducing the number of required measurements from 4096 to 128, which is a reduction by a factor of 32. The calculated matrix entries are upscaled to 255 so that the LED intensities cover the full available display range from 0 to 255. Fig. 1b) shows exemplary illumination matrices.

It should be mentioned that instead of using a DCT, a Discrete Fourier Transformation (DFT) could have been employed. The advantage of using a DCT is the faster decrease of the coefficients than the corresponding DFT coefficients. Furthermore, the DFT requires twice as many measurements to consider not only the negative parts, but also the positive and negative imaginary parts of the calculated matrices.

3. MATERIALS AND METHODS

3.1 Tissue Preparation

All measurements were performed on an unstained coronal section of a vervet monkey brain section with a thickness of $60\ \mu\text{m}$ that is embedded in 20% glycerin. The brain was removed from the skull within 24 hours after death and fixated with a buffered solution of 4% formaldehyde to prevent decay and stored at a temperature of 4°C . Then, the brain was immersed in a solution of 10% glycerin and then 20% glycerin for cryoprotection, each for several days. Afterward, the brain was frozen to a temperature of -80°C , cut into thin sections of $60\ \mu\text{m}$ with a large-scale cryostat microtome (*Leica Microsystems, Germany*) along the coronal plane, mounted onto glass slides, thawed, embedded in 20% glycerin, and finally cover-slipped and sealed for subsequent measurements.

3.2 Setup

Fig. 1a) sketches the measurement principle of Computational Scattered Light Imaging. The essential components are a light source that is capable to illuminate the sample under various angles, the tissue section and a camera. Additionally, adequate shielding from ambient light and stray light is required. A large LED display (*Absen Polaris 3.9pro In/Outdoor LED Cabinet*) with a size of $50\times 50\text{cm}^2$ was used as the light source. The LED display consists of 128×128 individually controllable RGB LEDs that have a pixel pitch of 3.9 mm. It achieves an overall brightness of $5000\ \text{cd}/\text{m}^2$ according to the manufacturer. Each illumination square consists of 2×2 pixels, resulting in a grid of $64\times 64 = 4096$ illumination squares in the pixel-based Euclidean illumination matrix. White RGB light was used for the measurements. The inner 12×12 LEDs right below the camera must remain dark for all illumination matrices as their direct brightness outshines the straylight signal. The tissue sample was placed on a specimen stage at a height of 17 cm above the center of the LED display. The maximum angle of incidence (that can be obtained from every azimuth, neglecting the corner LEDs) is therefore $\tan^{-1}(25\ \text{cm}/17\ \text{cm}) \approx 56^\circ$.

The camera (*SVS-VISTEK HR455CXGE*) has 9568×6380 pixels with a sensor size of $36\times 24\ \text{mm}^2$, resulting in a sensor pixel size of $3.76\times 3.76\ \mu\text{m}^2$. The above-average sensor pixel size results in a higher light sensitivity of the camera that has proven to be beneficial in Compressed Sensing, as slight intensity differences in the measured images can have a great influence on the Compressed Sensing evaluation. For the measurements, an entocentric objective was used (*Qioptiq OPTEM Lower Lens 1.25/160 mm*) with a focal length of 160 mm, an object-space resolution of $1.67\ \mu\text{m}/\text{px}$ and a field of view of $1.6\times 1.1\ \text{cm}^2$. The whole setup was thoroughly shielded from ambient light in a dark enclosure. Additionally, a black cone was mounted over the objective lens to prevent internal reflexes. A black paper mask was placed on the section, covering everything but the field of view, in order to prevent reflections from the glass surface of the specimen slide.

3.3 Gamma Correction

In contrast to the Euclidean illumination, wherein each LED exhibits either full intensity or is switched off, the Compressed Sensing illumination relies heavily on the correctly displayed color value of the illumination squares for the accurate reconstruction of scattering patterns. The relation between the displayed and the detected color value should ideally be linear. However, if a non-linear relationship exists, gamma correction is required and either the illumination matrices or the measured images need to be gamma corrected for the subsequent evaluation. Here, the gamma correction was applied directly to the displayed illumination matrix to prevent unpredictable error propagation in the measured images. To determine the appropriate factor for gamma correction, a series of 256 images with grey values ranging from 0 to 255 was generated and displayed on the LED screen. A plastic diffuser plate was placed on the specimen stage. The exposure time was selected such that the brightest gray value produces an intensity slightly below the point of overexposure, resulting in an exposure time of 350 ms with a gain of 3dB. To improve the Signal-to-Noise Ratio, two measurements were taken and averaged. The correction factor γ is defined by

$$I_{\text{out}} = p \cdot I_{\text{in}}^\gamma \quad (5)$$

with p being a fitting parameter. $\gamma = 2.641 \pm 0.008$ was determined using a least square fit as shown in Fig. 1c). The fitting range was limited to a gray value range from 35 to 235 to safely exclude any under- and overexposed pixels. The illumination matrices were then corrected using the inverse exponent $\gamma^{-1} = 0.38$.

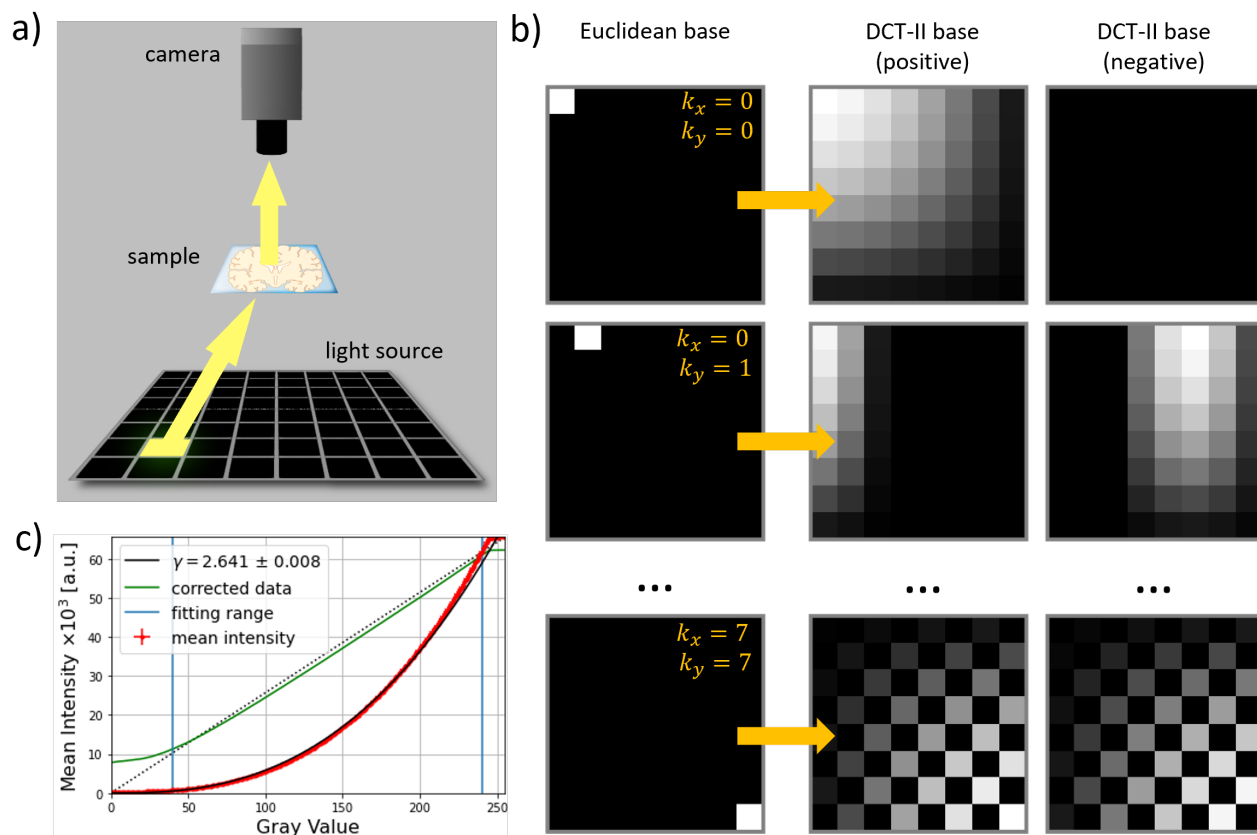


Figure 1. a) Sketch of ComSLI measurement. An illumination square or illumination image illuminates the sample under an angle. The camera detects the vertically scattered light from the sample. b) Euclidean illumination images are transformed to DCT-II illumination images by applying a two-dimensional DCT-II transformation to the illumination matrix. The transformed matrices are split up into two matrices, representing the positive and the negative values. This is required because it is impossible to illuminate with negative intensity values and results in twice as many illumination images when no further compression is applied. c) Gamma correction of the light source. The measured gamma factor must be applied to the illumination images so that all intensities are displayed correctly.

3.4 Tissue Measurements

For the measurement, a brain area was chosen that contains the parts of the corpus callosum, the corona radiata and the fornix. These regions were chosen due to their well-known fiber architecture, rendering them well-suited for initial studies of Compressed Sensing in ComSLI. The corpus callosum primarily contains flat, parallel, in-plane fiber bundles while the corona radiata is characterized by multiple interwoven fiber bundles that form distinctive fiber crossings. The fornix consists of inclined fibers, i.e. fiber orientations with an out-of-plane component.

Two ComSLI measurements were conducted: The first measurement employed Euclidean illumination, performing $64 \times 64 = 4096$ measurements for the image set with white RGB light, an exposure time of 1000 ms, a gain of 0 dB, an image depth of 16 bits. Each image is measured twice for averaging. The second measurement was performed with DCT illumination, resulting in $2 \times 64 \times 64 = 8192$ measurements with white RGB light. The exposure time for DCT illumination can be much lower because the patterns have a higher overall brightness than the Euclidean patterns. However, the exposure time decrease is not directly proportional because the number and intensity of illuminated squares varies for the DCT patterns. Therefore, the exposure time was chosen so that the brightest patterns do not lead to overexposure, leading to an exposure time of 400 ms, a gain of 0 dB, an image depth of 16 bits and averaging over 2 images.

3.5 Generation of Scattering Patterns

The measured images were processed as established by Menzel et al.:⁴ The scattering patterns for every pixel were generated by arranging the measured intensities in a 64×64 grid, corresponding to the order in the measurement. This was done for every 50-th pixel while averaging over a kernel of the 10×10 surrounding pixels. In case of the Euclidean illumination, the resulting 64×64 images represent the real-space scattering patterns for every evaluated kernel. The shape of the scattering pattern corresponds directly to the fiber orientations. To illustrate why it is not useful to reduce the amount of coefficients directly in the Euclidean measurement instead of using the more complex Compressed Sensing illumination, the Euclidean measurement was also downsampled from 64×64 pixels to 32×32 , 16×16 and 8×8 pixels for two exemplary scattering patterns.

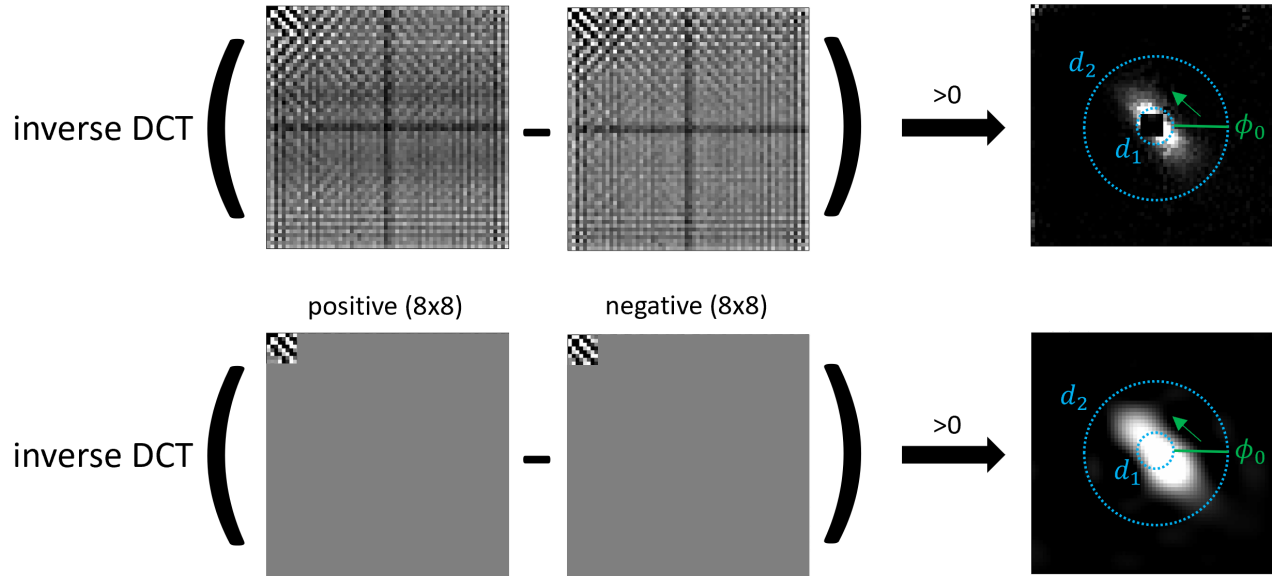


Figure 2. Reconstruction of Euclidean scattering patterns from DCT images. Two transformed scattering patterns of size 64×64 can be reconstructed from the DCT illumination, one from the positive illumination images and one from the negative illumination images. When the negative coefficients are subtracted from the positive coefficients and an inverse DCT-II is applied, the scattering patterns are reconstructed. In case of compression, all coefficients except for the first $N \times N$ (here: $N=8$) are zero. This results in a blurred scattering pattern. A polar integral is used to calculate the line profiles, leaving out the innermost and outer pixels (denoted with radii d_1 and d_2).

3.6 Reconstruction of DCT Scattering Patterns

In case of the DCT illumination, the positive and negative image sets were initially treated separately, using the same rearrangement procedure as in Euclidean illumination. The results are $2 \times 64 \times 64$ images per evaluated kernel, one derived from the positive DCT illumination, one derived from the negative DCT illumination. Those images contain both negative and positive values. In order to extract information regarding the fiber directions from those images, the real-space scattering patterns need to be reconstructed. Fig. 2 illustrates the algorithm for an exemplary scattering pattern from the corpus callosum: The intensity values of the negative DCT image were subtracted from the intensity values of the positive DCT image, resulting in an image that corresponds to the DCT transform of a scattering pattern obtained with Euclidean illumination.

In Compressed Sensing, the main objective is the reduction of required measurements, i.e. omitting higher-order illumination matrices from the measurement. To simulate the acquisition of measurements with fewer illumination matrices, all coefficients except for the first $N \times N$ coefficients were set to zero, being equivalent to a compressed measurement with a reduced number of illumination matrices. To demonstrate the capabilities

of compressing, this was done for 64×64 coefficients (that is, a full uncompressed measurement), 32×32 , 16×16 and 8×8 coefficients (Fig. 2).

An inverse DCT-II using the `scipy.fft` module can retrieve the corresponding real-space scattering pattern⁹ and was applied to every scattering pattern, both for the compressed and the uncompressed scattering patterns. Theoretically, the scattering patterns contain only positive intensity values. In practice, the calculated scattering patterns contain a portion of negative values. Therefore, only the positive intensity values were taken into account for the subsequent analysis. The result are compressed and uncompressed Euclidean illumination that contain direct information about fiber directions.

3.7 Generation of Line Profiles

The center of the scattering pattern shifts depending on the scattering pattern position in the field of view. For the correct calculation of the line profiles, this offset is corrected based on the distance between consecutively lit LED squares, and the pixel pitch of the optical setup. A polar integral is used to calculate the line profiles by summing up the pixel intensities going from an inner circle with diameter d_1 towards an outer diameter d_2 . The inner circle is large enough to contain the either dark (for Compressed Sensing illumination) or overexposed (for Euclidean illumination) pixels that are directly below the camera. The scattering pattern is sampled for 360 consecutive angles as shown in Fig. 2, starting at an angle $\phi_0 = 0^\circ$ and going counterclock-wise around a circle. To enable a comparison of the obtained line profiles, the intensity values were normalized using

$$I_{norm} = \frac{I - I_{min}}{I_{max} - I_{min}} \quad (6)$$

Subsequently, the line profiles were visualized by plotting the normalized intensity values against the corresponding angles ϕ , ranging from 0° to 360° in steps of 1° .

4. RESULTS

The subsequent sections present scattering patterns derived from three distinct brain regions characterized by their distinct nerve fiber orientations. These scattering patterns serve as examples for typical fiber orientations encountered in ComSLI, i.e. flat fibers, crossing fibers and inclined fibers, and as a demonstration of both the potential and the current limits of Compressed Sensing in ComSLI. As a reference, the first column shows the scattering pattern obtained through the Euclidean illumination patterns. Subsequent columns exhibit increasing degrees of compression, starting with the uncompressed DCT measurement (64×64) up to a highly compressed measurement with only 8×8 coefficients. Notably, the scattering patterns acquired from the DCT measurement feature a dark square in the image center corresponding to the cut-out in the original DCT illumination images. The intensity values are displayed with a viridis color map for better visualization. Additionally, line profiles for each scattering pattern in various stages of compression are provided for comparison.

4.1 Downsampling of Euclidean Illumination

To illustrate why the amount of measurements can not simply be reduced by reducing the Euclidean illumination from 64×64 squares to fewer squares, the Euclidean measurement was downsampled for two exemplary scattering patterns from the corona radiata and the corpus callosum, as shown in Fig. 4. While the pixels of the scattering pattern become larger, the characteristic features of the patterns start to disappear. The fiber directions and crossing are still recognizable in the 32×32 scattering pattern but lost with higher levels of reduction.

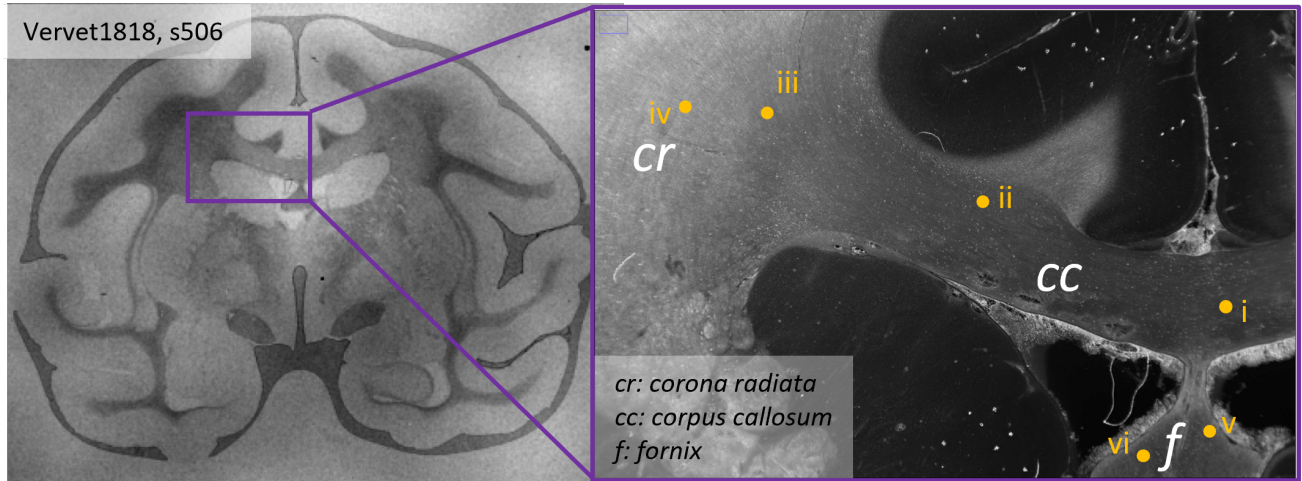


Figure 3. Coronally cut section (section no. s506) of a vervet monkey (Vervet1818) brain (left). For the evaluation, a region that contains parts of the corpus callosum (cc), the corona radiata (cr) and the fornix (f) has been chosen for the evaluation (right). These regions are exemplary for typical fiber orientations encountered in ComSLI, i.e. in-plane, parallel fibers in the corpus callosum (cc), crossing fibers in the corona radiata (cr) and parallel, out-of-plane fibers in the fornix (f).

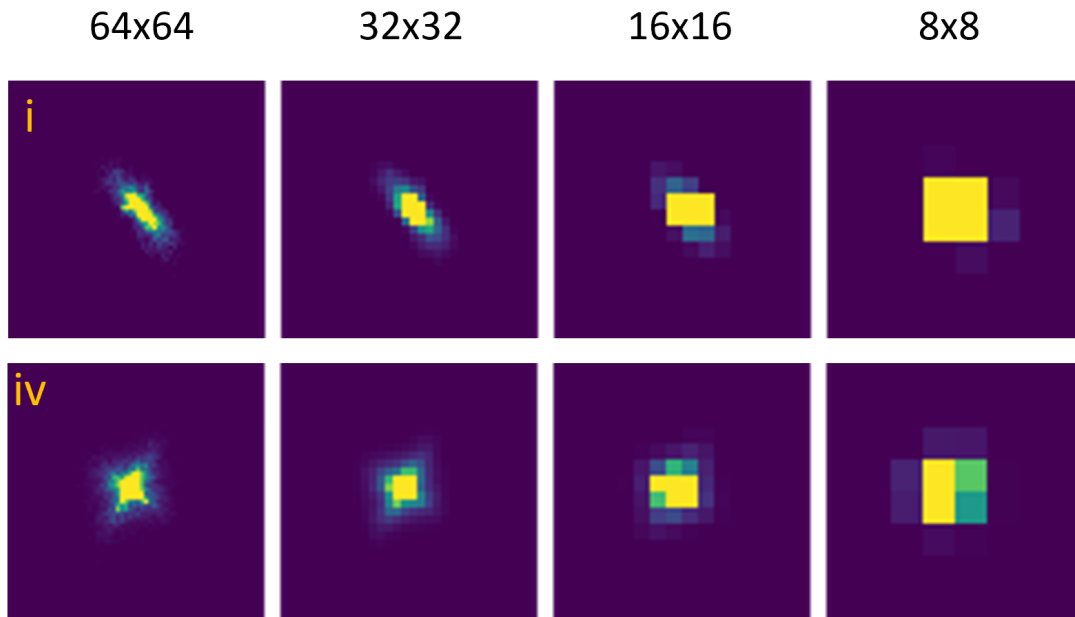


Figure 4. Scattering patterns for two exemplary kernels, one from the corpus callosum and one from the corona radiata. The Euclidean illumination matrix is downscaled, from the original 64×64 illumination squares down to only 8×8 illumination squares. The characteristic features of the scattering pattern (i.e. the fiber directions and crossings) are lost in the process; thereby demonstrating the need for a more complex approach to reduce measurement time and stored data.

4.2 In-Plane Parallel Fibers

The corpus callosum primarily contains flat, parallel, in-plane fiber bundles. The characteristic scattering patterns manifest as bar-shaped structures, with the long axis of the bar oriented orthogonally to the fiber direction. The two different directions in the left and right part of the corpus callosum are visible for the Euclidean illumination, but also up to the highest degree of compression. Although the bar blurs increasingly towards higher degrees of compression, the angular direction persists. This observation is supported in the line profiles where the two peaks broaden but keep their angular position at a distance of $\approx 180^\circ$, as expected for in-plane, parallel fibers. At higher compression levels, cross-shaped periodic artefacts along the x- and y-axis become visible but do not significantly influence the overall results.

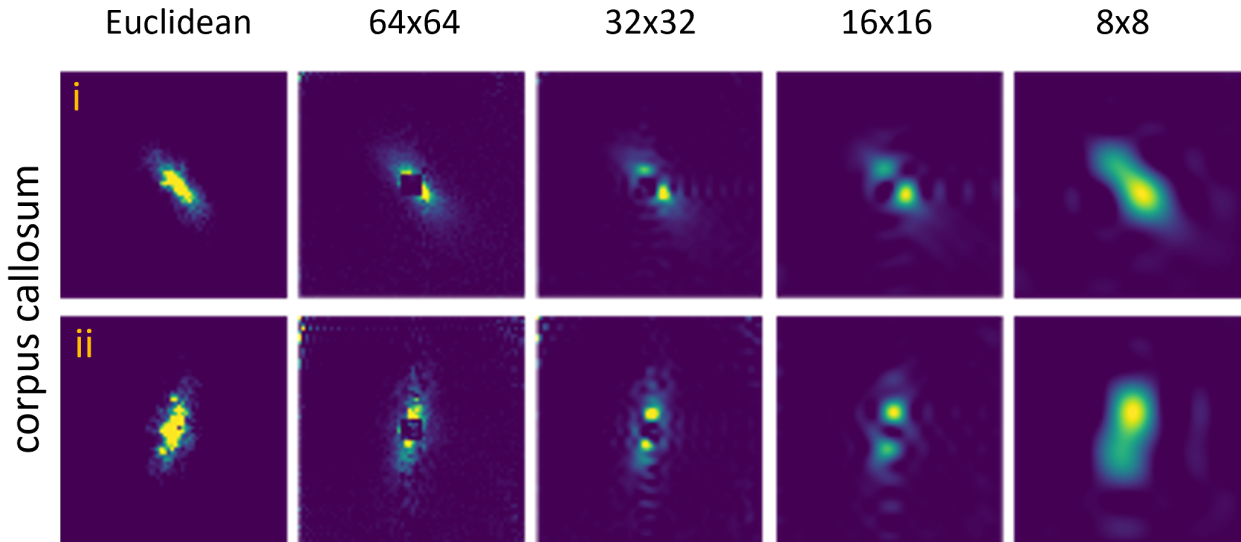


Figure 5. Scattering patterns for two exemplary kernels in the corpus callosum with increasing compression levels. The scattering pattern obtained with Euclidean illumination are shown as reference. The characteristic scattering pattern for in-plane, parallel fibers present themselves as bar-shaped structure where the long axis is oriented orthogonally to the fiber direction.

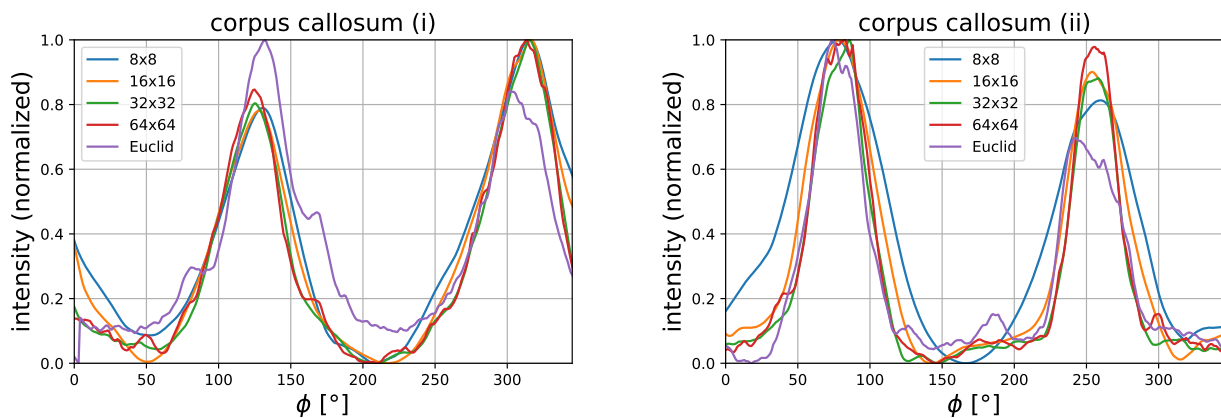


Figure 6. Line profiles calculated from the scattering patterns for the corpus callosum. Two peaks are obtained from the bar-shaped structure; the distance between the two peaks is $\approx 180^\circ$. The minima between the two peaks correspond to the fiber direction. The peaks broaden towards higher levels of compression but their angular position remains stable and discernible.

4.3 Crossing Fibers

The corona radiata is characterized by several crossing fiber bundles. The scattering patterns of a coronally cut brain section are dominated by two crossing in-plane fiber bundles that become visible as an X-shape. The two X-bars correspond again to two fiber directions that are orthogonally oriented to the long axis of each bar. The crossing angle matches up to the fiber bundles' crossing angle. The X-shaped configuration is discernible by the naked eye up to the highest compression levels even though the 8×8 scattering pattern has nearly lost its major directions. Yet, the evaluation of line profiles decreases in precision as the X-shape blurs, the peaks broaden and start to merge and shift as a result of blurriness. Again, artefacts associated with the compression become visible as periodic patterns along the x- and y-axis.

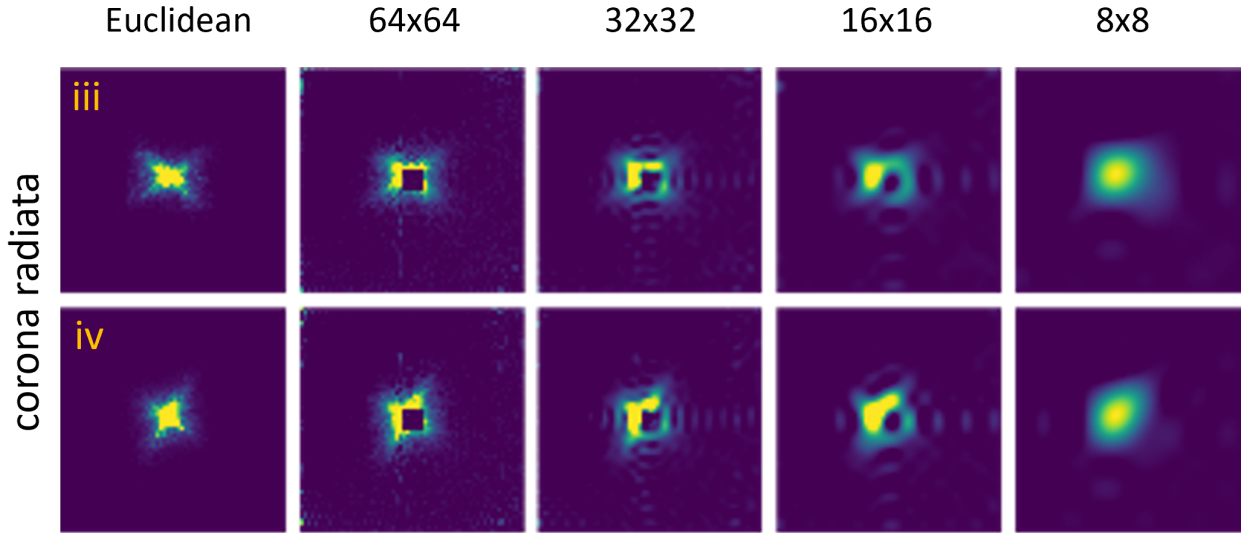


Figure 7. Scattering patterns for two exemplary kernels in the corona radiata with increasing compression levels. The scattering pattern obtained with Euclidean illumination are shown as reference. The characteristic scattering pattern for in-plane crossing fibers have an X-shape where the long axis of each crossing bar is oriented orthogonally to the fiber direction of one fiber bundle.

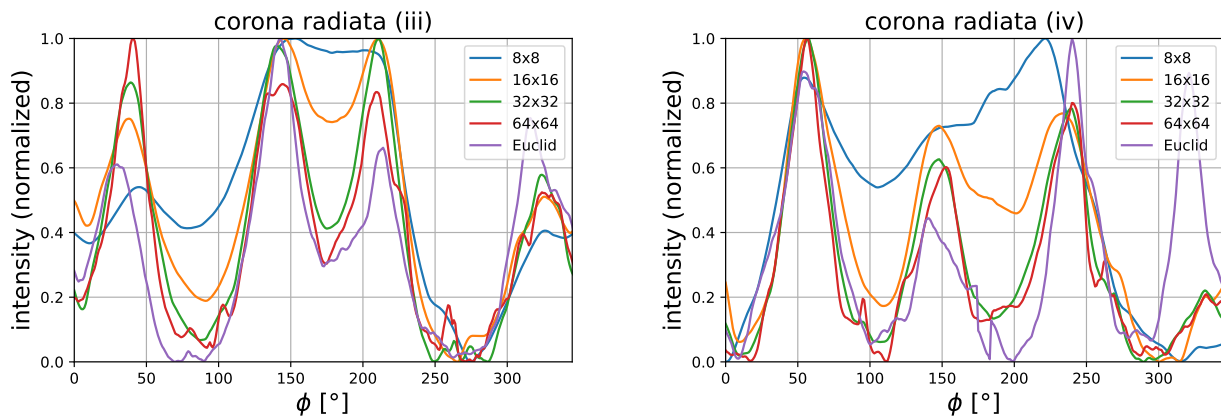


Figure 8. Line profiles calculated from the scattering patterns for the corona radiata. Four peaks correspond to the X-shaped structure of the corpus callosum and present two crossing fibers. Their angular position starts to shift and merge up to higher levels of compression.

4.4 Out-Of-Plane Fiber Inclinations

The fornix consists of inclined fibers, i.e. fiber orientations with an out-of-plane component. This manifests as a curvature of the bar-shaped scattering pattern that is characteristic for parallel in-plane fiber bundles. Two scattering patterns are shown where one exhibits a stronger curvature than the other one. As seen in the corpus callosum, the shape of the scattering pattern is stable in its general features such as direction and curvature. The curvature can be observed with the naked eye even up to the highest stage of compression. The line profiles yield distinct and similar peaks, with their distance deviation from 180° reflecting the curvature of the scattering pattern and thereby inclination. Again, the peaks broaden towards higher compression levels but the overall angular position remains stable. As before, compression artefacts are present.

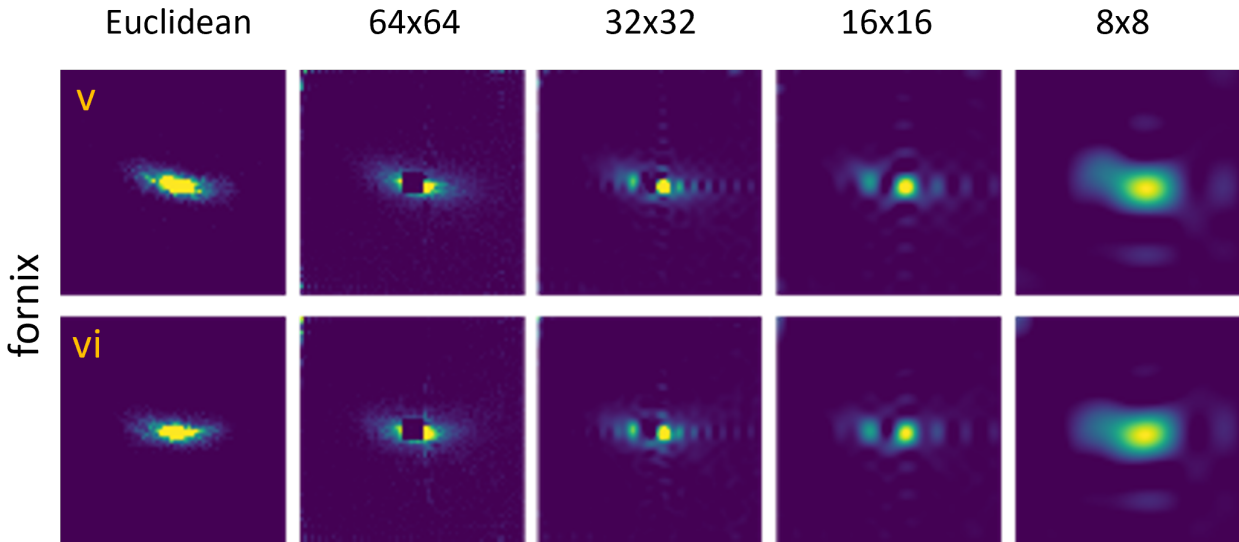


Figure 9. Scattering patterns for two exemplary kernels in the fornix with increasing compression levels. The scattering pattern obtained with Euclidean illumination are shown as reference. The characteristic scattering pattern for out-of-plane (i.e. inclined) parallel fibers shows a curvature that increases with higher inclination angles. The curvature can be seen with the naked eye up to the highest level of compression.

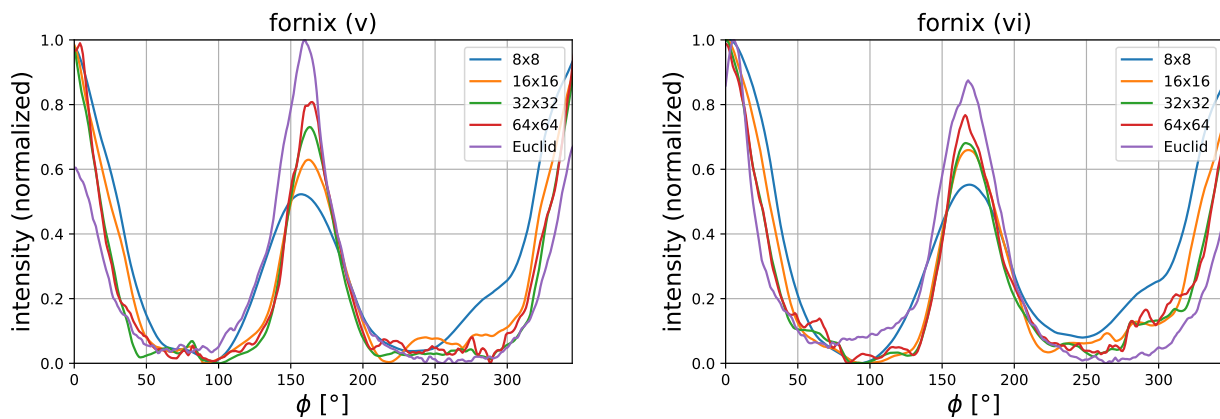


Figure 10. Line profiles calculated from the scattering patterns for the fornix. Two peaks correspond to the curved bar structure; the distance between the two peaks deviates from 180° and is related to the out-of-plane inclination of the fiber. The peaks broaden towards higher levels of compression but their angular position remains stable and discernible.

5. DISCUSSION

Initial results for various scattering patterns suggest that Compressed Sensing based on a DCT-II is applicable in ComSLI and feasible even for the highest investigated compression level of 8×8 . The possibility to retrieve fiber characteristics even from the most compressed scattering patterns shows the potential of Compressed Sensing. However, the algorithm for the quantitative evaluation of the pattern requires optimization, especially for crossing fibers. Those scattering patterns may be discernible with the naked eye, but the calculation of line profiles fails for the highest compression level and results in shifted and merging peaks. Machine learning approaches can be applied to improve recognition of scattering patterns that are difficult to analyze mathematically due to their compression-related blurriness.

Future studies should investigate the origin of the compression artefacts that become visible as periodical cross structures in the reconstructed compressed scattering patterns. Due to their symmetry, they may be a result of compressing the central black square that is caused by the cut-out in the illumination (otherwise, the black square has not yet shown any negative influence in the evaluation of the scattering patterns). Furthermore, the small amount of negative values in the reconstructed scattering pattern needs to be investigated. If these negative values stem from noise, a measurement with more repetitions may reduce them. Apart from that, they do not seem to cause any visible problems in the signal analysis if simply set to zero.

The main reason for a Compressed Sensing approach in ComSLI is the reduction of measurement time and stored data. Given that the scattering patterns are discernible at least by the naked eye up to the highest compression level and that there is still room to improve the quantitative evaluation of line profiles, even an 8×8 compression seems a realistic goal. However, it may be of interest to initially consider a less compressed measurement. Tab. 1 provides an overview of the required time and data for all stages of compression. For the DCT-II, twice as many measurements as coefficients are required for the reconstruction of scattering patterns, rendering an uncompressed (64×64) measurement pointless in comparison to the Euclidean measurement. Yet, a compressed measurement with 32×32 images or less starts to become beneficial. The factor 2 is taken into account in the second column of the table. The total measurement time is calculated under the assumption that only one measurement image is taken per illumination image (repetitions = 1), with no time required to process and store the image on the hard drive. Therefore, the total measurement time is an ideal lower limit. The actual measurement time depends on the measurement software and processing hardware. The real measurement time for the current setup is roughly twice as long as the theoretical lower limit. The total stored data assumes a single-channel image with a bit depth of 16 bit and an image size of 9568×6380 pixels. Furthermore, it does not take into account any further lossless compression of the measured images that may be applied to every image (e.g., an LZW (Lempel-Ziv-Welch) algorithm¹⁰). Generally, it is possible to subsequently reduce the size of the stored images using such an algorithm. The highest compression stage of 8×8 only requires 3% of data storage. In

Table 1. Estimated measurement time and data storage for various compression levels.

compression	images	exposure time	total time	data stored
Euclidean	4096	1000 ms	68 minutes	≈ 500 GB
64×64	8192	400 ms	55 minutes	≈ 1000 GB
32×32	2048	400 ms	14 minutes	≈ 250 GB
16×16	512	400 ms	3 minutes	≈ 62.5 GB
8×8	128	400 ms	> 1 minute	≈ 15.6 GB

terms of total measurement time, the benefit is even higher: Due to the brighter DCT illumination, the exposure time can be decreased, lowering the required measurement time down to only 1.5% of the original measurement time. Even an uncompressed 64×64 is - in theory - quicker than the original Euclidean measurement.

However, the Compressed Sensing method presents some drawbacks; mainly the need for a high-quality camera that is able to distinguish the subtle variations in intensity in the illuminated sample. Previous experiments with a lower-quality camera (*BASLER acA5472-17uc*) have not been successful. Furthermore, a bright display

and profound light shielding are absolutely required. So far, one of the strengths of ComSLI has been that measurements are already possible with relatively inexpensive hardware. It seems that Compressed Sensing has higher requirements upon the hardware.

6. CONCLUSION

In this paper, we presented the first steps towards implementing a Compressed Sensing application for Computational Scattered Light Imaging, highlighting both the potential and the current constraints of the method. The advantages of using a Discrete Cosine Transformation (DCT-II) were outlined and the mathematical background to generate the DCT-II illumination matrices from the standard Euclidean matrices was illustrated. First measurements were taken as a proof-of-concept for various scattering patterns from different characteristic brain regions. We found that it is possible to retrieve features like fiber directions, fiber crossings and fiber inclinations from the compressed scattering patterns that remain discernible up to the highest level of compression. Therefore, Compressed Sensing is a very promising approach to significantly reduce measurement time to only 1.5% of the originally required time and the stored data to 3% of the originally required data in ComSLI. Thus, Compressed Sensing opens the way to analyze a multitude features of the nerve fiber architecture with significantly lower time and storage requirements.

ACKNOWLEDGMENTS

We thank Roger Woods from the UCLA Brain Research Institute for providing the vervet brain sample (National Institutes of Health under Grant Agreements No. R01MH092311 and 5P40OD010965), the laboratory team from the Institute of Neuroscience and Medicine (INM-1), Forschungszentrum Jülich for preparing the brain section, and Philipp Schlömer for his support with the experimental hardware. This work was supported by the Helmholtz Association port-folio theme "Supercomputing and Modeling for the Human Brain", by the European Union's Horizon 2020 Research and Innovation Programme under Grant Agreement No. 945539 ('Human Brain Project' SGA3), the Klaus Tschira Stiftung gGmbH (Klaus Tschira Boost Fund), and the Deutsche Forschungsgemeinschaft (DFG) under Grant No. 498596755.

REFERENCES

- [1] Menzel, M., Reuter, J. A., Gräbel, D., Huwer, M., Schlömer, P., Amunts, K., and Axer, M., "Scattered light imaging: Resolving the substructure of nerve fiber crossings in whole brain sections with micrometer resolution," *NeuroImage* **233**, 117952 (2021).
- [2] auf der Heiden, F., Georgiadis, M., Zeineh, M., Amunts, K., Axer, M., and Menzel, M., "Reconstruction of nerve fiber orientations in cell-body stained histological brain sections using computational scattered light imaging," *BW1B.3* (Jan 2023).
- [3] Menzel, M. and Pereira, S. F., "Coherent Fourier scatterometry reveals nerve fiber crossings in the brain," *Biomed. Opt. Express* **11**, 4735–4758 (Aug 2020).
- [4] Menzel, M., Ritzkowski, M., Reuter, J. A., Gräbel, D., Amunts, K., and Axer, M., "Scatterometry measurements with scattered light imaging enable new insights into the nerve fiber architecture of the brain," *Frontiers in Neuroanatomy* **15** (2021).
- [5] Candès, E. J., Romberg, J. K., and Tao, T., "Stable signal recovery from incomplete and inaccurate measurements," *Communications on Pure and Applied Mathematics* **59**(8), 1207–1223 (2006).
- [6] Donoho, D., "Compressed sensing," *IEEE Transactions on Information Theory* **52**(4), 1289–1306 (2006).
- [7] Ahmed, N., Natarajan, T., and Rao, K., "Discrete cosine transform," *IEEE Transactions on Computers* **C-23**(1), 90–93 (1974).
- [8] Strang, G., "The discrete cosine transform," *SIAM Review* **41**(1), 135–147 (1999).
- [9] The SciPy community, "Fourier transforms (scipy.fft)." <https://docs.scipy.org/doc/scipy/tutorial/fft.html> (2023). [Online; accessed 6-November-2023].
- [10] Welch, "A technique for high-performance data compression," *Computer* **17**(6), 8–19 (1984).